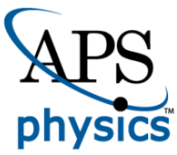

Regulation of biochemical reaction rates by flexible tethers

Daniel Reeves, Keith Cheveralls, and Jane Kondev

Phys. Rev. E **84**, 021914 — Published 10 August 2011

DOI: 10.1103/PhysRevE.84.021914

Regulation of biochemical reaction rates by flexible tethers

Daniel Reeves, Keith Cheveralls, and Jane Kondev*

Department of Physics, Brandeis University, Waltham, MA 02454

Abstract

We explore how ligand-receptor binding kinetics can be controlled by tethering the receptor to the end of a flexible polymer. The tether confines the diffusive motion of the receptor thus influencing the rate at which it captures ligands that are free in solution. We compute steady-state collision rates between ligand and receptor for this "tethered-capture" mechanism using a combination of analytic and numerical techniques. In doing so, we uncover a dimensionless control parameter, the "opacity", that determines under what conditions and to what extent a tether regulates the ligand-receptor collision rate. We compute the opacity for a number of different tethering scenarios that appear in biology and use these results to predict the affect of changing the length and flexibility of the tether on the rate at which ligands are captured from solution.

PACS numbers: 82.35.-x, 82.39.Rt, 87.15.kp

*Electronic address: kondev@brandeis.edu

I. INTRODUCTION

Polymer tethers play diverse roles in biological systems, from the regulation of ion channels to the assembly of viral capsids and actin filaments. This has inspired an extensive body of literature exploring how tether dynamics affects chemical reactions in which one or more of the reacting species is tethered by a flexible polymer [1–5]. For example, an interesting question is how viral capsid assembly is accelerated and stabilized by electrostatic interactions between the proteins that make the capsid subunits and the viral genome consisting of single stranded RNA. In one model, the RNA acts as an "antennae" to which protein subunits bind and then slide along to the growing capsid [6], thereby accelerating self-assembly. Structural studies [7] of yeast telomerase RNA, which maintains the integrity of the telomere regions of eukaryotic chromosomes, indicate that it contains binding sites for accessory proteins required for its function, that are separated from the central catalytic core. It has been suggested that the intervening RNA controls the rate of catalysis by serving as a flexible tether that connects the accessory proteins to the catalytic site. The cell adhesion literature explores how ligands tethered to the surface of one cell bind target receptors on neighboring cells. Theoretical work has stressed specific adhesion between surfaces, and includes equilibrium calculations for surface coating densities [8], and kinetic calculations in which one species is assumed stationary [9–11]. All have found that equilibrium and kinetic properties depend strongly on polymer parameters, such as length and flexibility. The same principles apply to polymer surface preparations that are relevant to many single molecule experiments. For example, one way to measure binding and unbinding kinetics using single molecule microscopy is to label the reactants with fluorescent dyes, confine one species by tethering it to the slide surface, and observe the other reactant binding and unbinding by detecting colocalization of the two fluorescent markers [12].

We propose that controlling the polymer properties of a tether that spatially confines a receptor can serve as a mechanism to regulate the rate at which it binds ligands. We expect a receptor at the end of a flexible polymer to bind ligands faster than a completely immobilized receptor, because the receptor is free to search the local region for the ligand; the length and flexibility of the tether control the speed and extent of the receptor's search. Previous work [6] focused on binding to an enlarged target provided by the long antennae, followed by 1D diffusion along that antennae. This distinct mechanism is equivalent to that

proposed for enhanced binding of transcription factors to target DNA. Berg and coworkers [13], developed theory for how transcription factors enhance targeted binding rates by weakly binding to DNA via a 3D diffuse search, followed by a 1D "sliding" search along the DNA. Our proposed mechanism focuses on dynamics of diffusing flexible tethers rather than the dimensionality of the search techniques.

A particularly illustrative case of tethered-capture occurs in formins, a widely-expressed family of proteins that are responsible for rapid nucleation and assembly of actin filaments and networks. By capping the fast-growing barbed end of actin filaments, formins exclude other capping proteins from halting the growth of the filament while still allowing insertion of actin subunits [14]. It has been proposed that flexibility of a tether-like FH1 domain and the presence of binding sites for actin-profilin complexes on that domain are the principal elements of the FH1 domain's function [15]. A two-step "capture and transfer" mechanism has been proposed [15] in which the FH1 domain serves as a flexible tether which first binds profilin-actin complexes and then transfers them to the growing filament end (see Fig. 1).

With these biological systems as motivation, we investigate how confinement of molecules by tethers affects reaction rates by considering reaction-diffusion models with simplified geometries and interactions. We will make use of the extensive body of literature devoted to the theory of polymer dynamics [16–21], and calculate binding rates following many of the same general ideas as those employed to arrive at the the Smoluchowki rate constant, $k_{\mathrm{S}} = 4\pi(D_r + D_l)R$, where D_r and D_l are the diffusion constants of the receptor and ligand, respectively, and R is the radius of interaction [22]. The difference in our work, compared to this canonical case, is that the receptor motion is limited by a flexible polymer leash.

The tethered-capture mechanism modifies the speed of a diffusion-limited reaction. Completely immobilizing the receptor reduces D_r to zero, thus reducing k_{S}. If the confinement is relaxed, perhaps by attaching the receptor to a short tether, we expect its limited motion to contribute to the reaction rate. A completely liberated receptor, with diffusion constant D_r, will increase the reaction rate over that of an immobilized receptor by a factor of $(D_l+D_r)/D_l$. The reaction rate will be between these two extremes for molecules undergoing tethered dynamics, which we model in two ways (see Fig. 2). In the first model, the receptor diffuses freely in a confining potential, which is chosen to act as a proxy for the polymer tether, a method previously employed in studies of polymer cyclization kinetics [20, 21]. In the second model, we consider explicitly the tether as an anchored bead-and-spring polymer

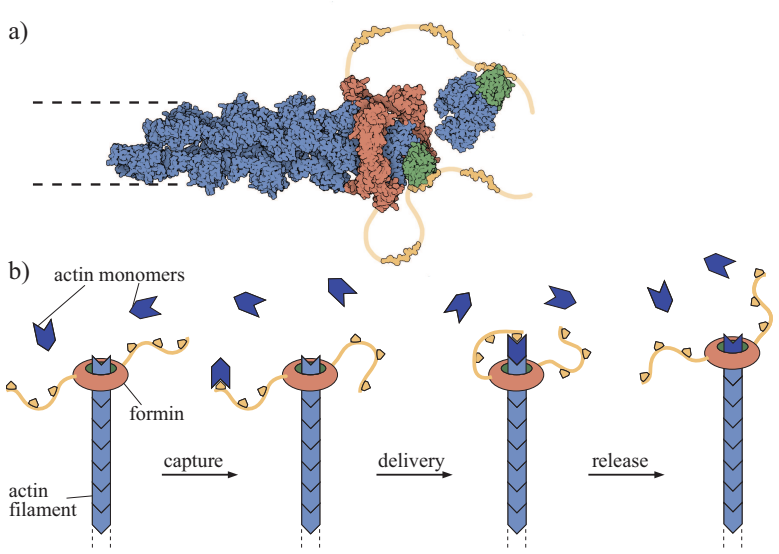

FIG. 1: (Color online) a) A structural model of the actin binding protein formin. b) A cartoon of formin-assisted actin polymerization. Diffusing actin monomers (*pointed shapes*) preferentially bind to the barbed end of the growing filament. The barbed end is capped by the FH2 domains of a formin protein dimer, from which extend tentacle-like FH1 domains that are decorated with actin binding sites. Having captured the actin monomers, the flexible tethers deliver them directly to the growing end. The tether domain unbinds from the actin, and the actin filament is elongated by one monomer length.

that undergoes Rouse dynamics, the terminal node of which is the receptor.

Both approaches lead to the same qualitative results regarding how the capture rate depends on the length of the tether and to a simple intuitive picture based on the comparison of two characteristic time scales. The first timescale is $\tau_D = \mathcal{R}_{\rm ee}^2/D_l$, the characteristic time for a ligand with diffusion constant D_l to diffuse over a sphere of radius $\mathcal{R}_{\rm ee}$, the root-mean-squared end-to-end distance of the polymer, which is the characteristic size of the region explored by the tethered receptor. The second time scale is $\tau_R = \frac{4}{3}\pi\mathcal{R}_{\rm ee}^3/k_{\rm mix}$, which is the characteristic binding time for ligands at the concentration of one ligand per volume of the sphere to which the receptor is confined. Here, $k_{\rm mix}$ is the ligand-receptor binding rate constant when both are free in solution. This so-called second-order rate constant has units of inverse time and inverse concentration, and when multiplied by the concentrations of the receptors and ligands, assumed to be uniform in solution, gives the rate of ligand-receptor complex formation.

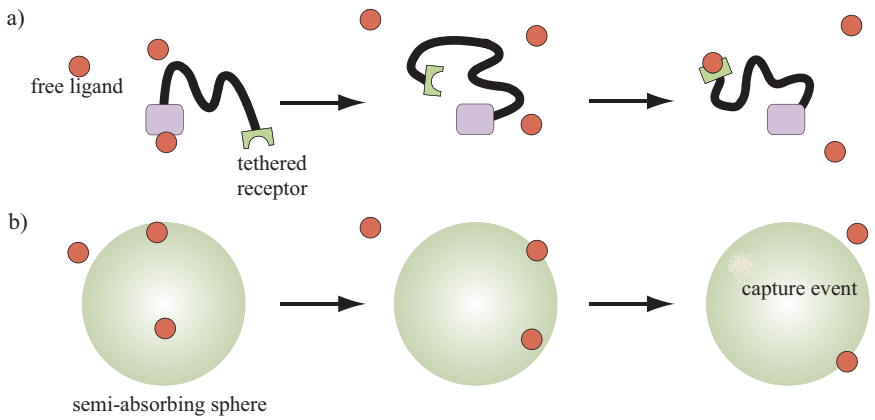

FIG. 2: (Color online) Schematic of two models for tethered capture. a) We explicitly model the tether as an anchored bead-and-spring polymer that undergoes Rouse dynamics, the terminal node of which is the receptor. b) While the ligand is allowed to diffuse freely everywhere, the receptor is confined within a spherical potential. The potential effectively distributes the receptor's concentration throughout the sphere.

When the ratio of these two times, $\sigma^2 = \tau_D/\tau_R$ is very large ($\sigma \gg 1$) then every ligand that stumbles into the sphere by random diffusion binds to the receptor. In this case, if c_l is the concentration of ligands in solution, we recover the Smoluchowski result, k_{S}, except now the size of the receptor is replaced by the typical end-to-end distance of the polymer tether. In the other limit, $\tau_D/\tau_R \ll 1$, ligands pass through the confining sphere without reacting, and the reaction rate constant approaches that of a well mixed solution of ligands around a receptor, $k_{\mathrm{cap}} \approx k_{\mathrm{mix}}$. We explore this "opacity" parameter, σ in more depth in Section IV.

Goals and approach

The general goal of this paper is to establish predictions for how confining receptors affects the rate of diffusion-limited binding of ligands. There are different types of confinement, and although we focus on confinement by tethers, we touch on and derive results relevant to confinement of a receptor to a region of space. The latter is similar to two-dimensional confinement to membranes, which has been studied extensively [23, 24]. Specifically, we predict how steady-state binding rates depend upon parameters such as the length and flexibility of a polymer tether, which limits the motion of a receptor molecule. We develop a hierarchy of models that embody different levels of approximations for the dynamics of the

tether and compare their predictions to computer simulations that serve as our benchmark.

In the following section we approximate tethered-capture using a potential of mean force or a hard-wall potential confining the receptor. The analytic solutions for this model has the advantage of uncovering the important dimensionless parameter σ whose value discerns between two regimes, one in which the reaction rate is not influenced by the presence of a tether and another in which it is sensitive to tether properties such as the persistence length and total contour length. In Section III we find numerical and approximate analytical solutions to the tethered capture rate while incorporating polymer dynamics of the tether. We find that although the attractive potential model does not capture in quantitative detail the effect of the tether on the rate of capture of ligands by the receptor, the value of the intuition and dimensionless parameter derived via the simpler theory is supported by the more sophisticated calculations. The simple analytic solutions guide us in drawing qualitative predictions for how tether properties affect kinetics in a number of synthetic and naturally occurring biological systems that can be readily tested in experiments. These are discussed in Section IV A.

There are several prevailing assumptions throughout this paper which are consistent with our goal of building the simplest model that captures the essential physics. First, we ignore all hydrodynamic effects on the diffusive motion of the polymer tether, which affects the dynamics, but allows for simpler theoretical analysis and simulations. The ommition of hydrodynamic effects removes correlations in the dynamics, and tends to lead to overestimation of binding rates [25]. Second, we ignore rotational alignment of ligand and receptor. The implications of this assumption and ways to treat rotational alignment have been explored elsewhere [26].

II. CONFINEMENT OF RECEPTORS BY AN ATTRACTIVE POTENTIAL

In this section we investigate receptors freely diffusing in an attractive potential. Although we primarily use the potential to model the effect of a polymer tether, the attractive potential model poses an interesting problem in its own right. For example, a hard-wall potential could model the compartmentalization of receptors inside cells. Or, the potential could represent the full extension of a mobile tether confining a very slow receptor. In the latter case the dynamics of the slow receptor are decoupled from the tether dynamics, and

the tether simply serves to limit the space available to the receptor. Free diffusion in a mean-force potential has been used as an effective model of polymer cyclization [20, 21], where the ligand and receptor are fixed to the two ends of a diffusing polymer chain. The mean-force potential in this case captures the effect of the polymer by recreating the correct equilibrium distribution of end-to-end distances.

A. Reaction-diffusion system in an external potential

Here we consider a reaction-diffusion systems of equations that describe the deterministic time-evolution of the receptor and ligand particle concentrations, $c_r(\mathbf{r},t)$ and $c_l(\mathbf{r},t)$. The ligands freely diffuse and are removed from solution upon colliding with the receptor. The receptor undergoes free diffusion in the confining potential, $U(r)$, and is likewise removed from solution upon interacting with a ligand. The resulting reaction-diffusion system of equations is

$$\begin{aligned}\frac{\partial c_r(\mathbf{r},t)}{\partial t} &= D_r\nabla^2 c_r(\mathbf{r},t) + \frac{1}{\xi}\nabla\cdot\left(c_r\left(\mathbf{r},t\right)\nabla U\left(\mathbf{r}\right)\right) - \int_V k_{\text{int}} S(r') p_{lr}(\mathbf{r},\mathbf{r}+\mathbf{r}',t)\,\mathrm{d}\mathbf{r}' \\ \frac{\partial c_l(\mathbf{r},t)}{\partial t} &= D_l\nabla^2 c_l(\mathbf{r},t) - \int_V k_{\text{int}} S(r') p_{lr}(\mathbf{r},\mathbf{r}+\mathbf{r}',t)\,\mathrm{d}\mathbf{r}', \end{aligned} \tag{1}$$

where $\xi = k_B T/D_r$ is the friction coefficient of the receptor. The joint particle density $p_{lr}(\mathbf{r},\mathbf{r}+\mathbf{r}',t)$ gives the probability of finding a ligand and receptor at $\mathbf{r}$ and $\mathbf{r}+\mathbf{r}'$ respectively. The rate constant k_{int} gives the rate at which ligands react with the receptor when within the reactive region defined by $S(r')$, which is centered on the receptor. For example, an absorbing sphere of radius R_{abs} is modeled by $S = \Theta(|\mathbf{r}'| - R_{\text{abs}})$ where Θ is the Heaviside (step) function. Fortunately, if R_{abs} is smaller than the length scale over which the potential changes, we can simplify the interaction terms to the more tractable and intuitive expression $k_{\text{mix}} c_r c_l$ [22]. The diffusion-limited second-order rate constant, k_{mix}, is the rate constant measured for a well-mixed solution of free reactants. This identification agrees with the limiting case of no confining force and spatially uniform concentrations, in which case the gradient terms vanish and we recover the usual kinetic rate equations (e.g. $\partial c/\partial t = -k_{\text{mix}} c_r c_l$). For further discussion of these identifications and the conditions under which the approximations break down, see Ref. [22].

In the following section, we determine binding rates between ligands and receptor by calculating the steady-state rate of ligands passing through a sphere of size R much larger

than the characteristic size of the tether. This capture rate is computed from the steady state ligand concentration, which is assumed to be fixed and equal to C_0 in the far field. Under this steady-state condition, the coupled diffusion reaction equations are,

$$\begin{aligned}\frac{\partial c_r(r)}{\partial t} &= D_r\nabla^2 c_r(r) + \frac{1}{\xi}\nabla\cdot(c_r(r)\nabla U) - k_{\mathrm{mix}}c_r(r)c_l(r) = 0\\ \frac{\partial c_l(r)}{\partial t} &= D_l\nabla^2 c_l(r) - k_{\mathrm{mix}}c_r(r)c_l(r) = 0.\end{aligned} \tag{2}$$

The capture rate is given by the flux of ligands through a sphere larger than the reach of the receptor. This diffusive flux is proportional to the gradient of $c_l(r)$, which we divide by the far-field concentration C_0 to find the second-order tethered-capture rate constant, k_{cap}.

B. Analytic solutions

To apply a potential as a proxy for tethered confinement we use the mean-force potential $U_{\mathrm{mf}}(\mathbf{r})$ that preserves the correct equilibrium statistics for the position of the receptor. Our use of diffusion in a mean-force potential to approximate polymer dynamics is equivalent to the local equilibrium approximation (LEA) developed for polymer cyclization [20]. The LEA is valid in the limit when the relaxation time of the polymer is much less than the time scale of interest. In this case, the dynamics of the end-to-end vector are well described by a particle diffusing in the mean-force potential $U_{\mathrm{mf}}(\mathbf{r})$. In Appendix A we discuss how the LEA is applied to our model and the conditions under which the approximation holds.

For an ideal chain consisting of N statistical segments of length b, the equilibrium distribution of the end-to-end vector is

$$c_{\mathrm{eq}} = \left(\frac{3}{2\pi\langle R_{\mathrm{ee}}^2\rangle}\right)^{3/2}\exp\left(\frac{-3r^2}{2\langle R_{\mathrm{ee}}^2\rangle}\right), \tag{3}$$

where the mean-square end-to-end distance of the polymer is $\langle R_{\mathrm{ee}}^2\rangle = Nb^2$. The mean-force potential that preserves this equilibrium distribution must satisfy $U_{\mathrm{mf}}(\mathbf{r}) = -k_bT\log\left(c_{\mathrm{eq}}(\mathbf{r})\right)$, and is therefore harmonic:

$$U_{\mathrm{mf}}(r) = k_bT\frac{3r^2}{2\langle R_{\mathrm{ee}}^2\rangle}. \tag{4}$$

We now make several simplifications to find analytic solutions to Eqs. 2 with this confining potential. The first is a "weak interaction" assumption that decouples the differential equations by omitting the coupling term, $k_{\mathrm{mix}}c_lc_r$, from the equation of motion for the receptor concentration, while retaining it in the equation of motion for ligand concentration.

We employ scaling arguments in Appendix B to show that this assumption is valid when

$$\frac{\langle R_{\rm ee}^2 \rangle}{D_r} \ll \frac{1}{k_{\rm mix} C_0}. \tag{5}$$

Intuitively, this condition, which is satisfied in sufficiently dilute solutions, requires the receptor to explore the region to which it's confined faster than ligand binding. In this case, the spatial distribution of the receptor is returned to equilibrium much faster than the rate at which it is disturbed by interactions.

With the decoupling approximation, c_r maintains the equilibrium distribution given by Eq. 3. Fig. 3 gives numerical solutions for the apparent second-order rate constant $k_{\rm cap}$ for both the decoupled (*squares*) and coupled (*dots*) systems of equations, where we apply the potential $U_{\rm mf}(r)$ and set $D_r = D_l = 1\ \mu{\rm m}^2/{\rm s}$, and $k_{\rm mix} = 0.1\ \mu{\rm m}^3/{\rm s}$, parameters that are relevant for molecular biological systems [27]. Figure 3 supports the decoupling conditions given by Eq. 5. We have also confirmed (data not shown) that the equilibrium distribution of a self-avoiding chain produces approximately the same results.

The decoupled reaction-diffusion equations still lack analytic solutions. However, by approximating the quadratic potential with a hard-wall potential of width $R = \phi \mathcal{R}_{\rm ee}$, where $\mathcal{R}_{\rm ee} = \sqrt{\langle R_{\rm ee}^2 \rangle}$, the receptor density c_r becomes uniform within a sphere of radius R. Assuming spherical symmetry, we now have the tractable differential equations

$$\begin{aligned} 0 &= D_{\rm l} \nabla^2 c_l - \frac{k_{\rm mix} c_l}{\frac{4}{3}\pi R^3} \quad 0 < r < R, \\ 0 &= D_{\rm l} \nabla^2 c_l, \qquad r > R. \end{aligned} \tag{6}$$

We solve Eq. 6 for c_l subject to several simultaneous boundary conditions. The first implements a fixed concentration of ligands, C_0, far from the bound receptor. The second normalizes the receptor concentration such that there is exactly one receptor in the system. The last guarantees continuity of the ligand concentration at the origin and at $r = R$. The rate constant is

$$\begin{aligned} k_{\rm cap} &= 4\pi D_l R \left(1 - \frac{\tanh(\sigma)}{\sigma} \right), \\ \text{where} \quad \sigma &= \sqrt{\frac{3 k_{\rm mix}}{4\pi D_l R}}. \end{aligned} \tag{7}$$

The numerical comparison given in Fig. 3 confirms that a hard wall potential of radius $R \approx \phi \mathcal{R}_{\rm ee}$ is a good approximation to the mean-force potential $U_{\rm mf}(r)$ for $\phi = 1.3$. This

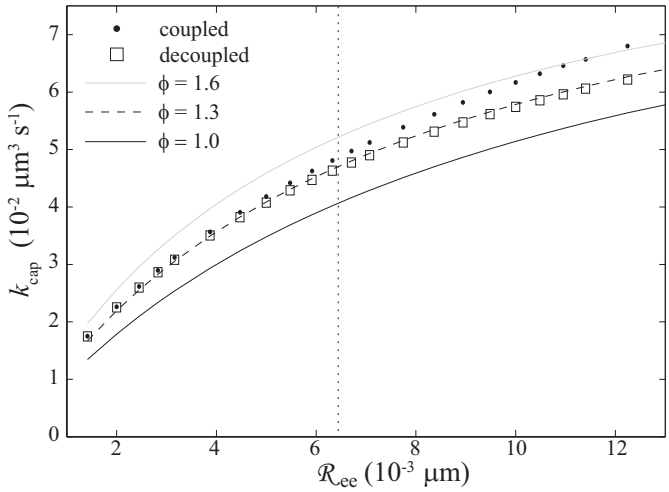

FIG. 3: Calculated apparent second-order rate constant, $k_{\rm cap}$, as a function of the characteristic size of the tether, $\mathcal{R}_{\rm ee}$. The rate constant is computed for the three models discussed in the text assuming model parameters $D_{l,r} = 1\mu m^2/s$, $k_{\rm mix} = 0.1\mu{\rm m}^3/{\rm s}$, and $C_0 = 10^4\mu{\rm m}^{-3}$: the harmonic potential model with coupling given in Eq.2 (*dots*), the uncoupled approximation of Eq. 2(*squares*), and the spherical hard-wall potential model given in Eq.7 (*lines*). Each line corresponds to a sphere of size $R = \phi\mathcal{R}_{\rm ee}$, for which we use three values to illustrate the sensitivity to the choice of ϕ. A spherical hard wall offers a good approximation to the decoupled harmonic potential when $\phi = 1.3$. Our theory predicts that for values of $\mathcal{R}_{\rm ee}^2 < D_r/C_0k_{\rm mix}$, the weakly interacting condition is satisfied and the decoupling approximation should be valid. That inequality is satisfied for $\mathcal{R}_{\rm ee} < 32\mu m$, and the vertical dotted line is placed at 0.2 of that limiting value.

factor is independent of model parameters. It is slightly larger than unity, indicating that the size of an absorbing sphere equivalent to a Gaussian sink is slightly larger than $\mathcal{R}_{\rm ee}$.

III. CONFINEMENT OF RECEPTORS BY A FLEXIBLE TETHER

In this section, we model a single receptor as the terminal node of a polymer, and compute reaction rates using both approximate analytic calculations and simulations. As before with the simpler potential model, we compute formulas for how the rate varies with polymer length.

A. Analytical results for tethered capture

To produce approximate solutions for binding rates with tethered diffusion we use techniques developed by Wilemski and Fixman [17] in the context of polymer cyclization. We start by adopting a coordinate system centered on the receptor, such that $\mathbf{r} = \mathbf{r}_l - \mathbf{r}_r$ is the position vector of the ligand with respect to the receptor. Because in this model the receptor does not freely diffuse, but rather undergoes more complicated motion that is coupled to all segments of the polymer, we can not express the time evolution of this position vector using a single differential equation as in Eq. 1. Rather, we write the time evolution using operator notation, where $\partial c_l(\mathbf{r},t)/\partial t = \mathcal{D}c_l(\mathbf{r},t)$ describes the diffusion of a ligand with respect to the diffusing tethered receptor, in the absence of ligand-receptor interactions. With interactions, the concentration of ligands follows the generalized reaction-diffusion equation,

$$\frac{\partial c_l(\mathbf{r},t)}{\partial t} = \mathcal{D}c_l(\mathbf{r},t) - k_{\text{int}}S(\mathbf{r})c_l(\mathbf{r},t). \tag{8}$$

Again, we let the ligand and receptor react when the distance between their centers is less than R_{abs}, so $S(\mathbf{r}) = \Theta(|\mathbf{r}| - R_{\text{abs}})$. To simplify the calculations, we assume a perfectly absorbing surface by solving Eq. 8 for finite k_{int} and then taking the limit $k_{\text{int}} \gg k_{\text{cap}}$. Our goal is to calculate the steady-state reaction rate $k_{\text{cap}} = \int d^3\mathbf{r}\, k_{\text{int}}S(\mathbf{r})c_l(\mathbf{r})$ where the ligand concentration has relaxed to steady-state and the far-field concentration is fixed at C_0.

The Wilemski-Fixman (WF) theory approximates solutions to Eq. 8 by steps outlined in Ref. [17]. We extend the approximation to give the steady-state reaction rate for a ligand reacting with a tethered receptor. In the fully absorbing limit where $k_{\text{int}} \gg k_{\text{cap}}$, the WF formula for the second order rate constant is

$$k_{\text{cap}} = \frac{\nu_{\text{ss}}^2}{C_0 \int_0^\infty dt\, Q(t)}, \tag{9}$$

where $\nu_{\text{ss}} = 4\pi R_{\text{abs}}^3 C_0/3$ is the expected number of ligands inside the reactive region in the well-mixed state. $Q(t)$ is the average number of ligands that are in the reactive region at both the initial time $t = 0$ and at time t,

$$Q(t) = \iint d\mathbf{r}d\mathbf{r}_0 S(\mathbf{r})G(\mathbf{r},\mathbf{r}_0,t)S(\mathbf{r}_0)C_0. \tag{10}$$

Here, $G(\mathbf{r},\mathbf{r}_0,t)$ is the Green's function, or propagator, for the ligand-particle separation, which is initially $\mathbf{r}_0$.

To understand Eq. 9 intuitively, we rewrite the first order rate $k_{\text{cap}}C_0$ as the ratio ν_{ss}/T, where $T = \nu_{\text{ss}}^{-1} \int dt Q(t)$. We interpret the time T as the total time a particle spends inside the sink before diffusing back into solution [18]. Since ν_{ss} ligands are absorbed by the sink every time interval T, the reaction rate is nothing but the ratio of these two quantities, which is equivalent to Eq. 9.

To find the Green's function, we begin by calculating the mean and variance of $\mathbf{r}(t)$ using the statistical independence of $\mathbf{r}_r$ and $\mathbf{r}_l$:

$$\begin{aligned} \langle \mathbf{r}(t) \rangle &= \mathbf{r}_0, \\ \text{var}(r(t)) &= \left\langle \mathbf{r}_r^2(t) \right\rangle + \left\langle \mathbf{r}_l^2(t) \right\rangle - \mathbf{r}_0^2 = \left\langle \mathbf{r}_r^2(t) \right\rangle + 6D_l t, \end{aligned} \tag{11}$$

where $\mathbf{r}_0 = \mathbf{r}_r(0) - \mathbf{r}_l(0)$. The value $\langle \mathbf{r}_r^2(t) \rangle$ is the mean-squared displacement as a function of time for the terminal bead of an anchored polymer. We model the polymer as a discrete Rouse chain made of N beads, each with the same diffusion constant as the terminal receptor, D_r, connected by springs of mean squared length b^2. We derive $\langle \mathbf{r}_r^2(t) \rangle$ in Appendix D using the normal-mode decomposition of $\mathbf{r}_r(t)$ [28]. This yields

$$\left\langle \mathbf{r}_r^2(t) \right\rangle = \sum_{p=1}^{N-1} \frac{2b^2}{2N-1} \cot^2 \left[\frac{(2p-1)\pi}{2(2N-1)} \right] (1 - e^{-t/\tau_p}), \tag{12}$$

where the relaxation time of the pth Rouse (normal) mode, τ_p, is

$$\tau_p = \frac{b^2}{12 D_r \sin^2 \left(\frac{\pi(2p-1)}{2(2N-1)} \right)}. \tag{13}$$

Because $\mathbf{r}_r$ is a linear combination of harmonic Rouse modes which are Gaussian distributed, and $\mathbf{r}_l$ is diffusive and therefore also Gaussian, the Green's function for $\mathbf{r}$ is Gaussian, and therefore completely determined by its mean and variance:

$$G(\mathbf{r}, \mathbf{r_0}, t) = \left(\frac{3}{2\pi \text{var}(r(t))} \right)^{-3/2} \exp \left(\frac{-3(\mathbf{r}(t) - \mathbf{r}_0)^2}{2\text{var}(r((t))} \right). \tag{14}$$

Evaluating the integral in Eq. 10,

$$\begin{aligned} Q(t) =& C_0 \frac{4}{3} \pi R_{\text{abs}}^3 \left[\text{Erf} \sqrt{\frac{6a^2}{\text{var}(r(t))}} + \right. \\ &\left. + \frac{1}{3R_{\text{abs}}^3} \sqrt{\frac{\text{var}(r(t))}{6\pi}} \left(\text{var}(r(t)) - 9R_{\text{abs}}^2 + (3R_{\text{abs}}^2 - \text{var}(r(t)) e^{\frac{-6R_{\text{abs}}^2}{\text{var}(r(t))}} \right) \right]. \end{aligned} \tag{15}$$

Equations 9 and 15 are the key results of the WF theory that we use to compute binding rate constants. Note that although the WF closure approximation (which is central in deriving Eq. 9) is nominally applicable only for small $k_{\rm int}$, it has been shown to give good results even for large $k_{\rm int} \gg k_{\rm cap}$ with an error of roughly 20% for many applications [18, 29].

B. Simulations of tethered-receptor ligand binding

To test the analytic approaches described in the previous sections, we have simulated the interactions between free ligands and a tethered receptor using off-lattice Monte-Carlo dynamics. Details on how these simulations are performed are found in Section C. Simulation results for $k_{\rm cap}$ for a representative parameter set are given in Fig. 4. Second order reaction rates, as given by simulation data (*black line*) and WF theory (*broken line*), are plotted as functions of tether length. Solving Eq. 9 exactly for the zero length tether case ($N = 1$) gives a result which deviates by a factor of 5/6 from the exact solution, $k_{\rm S} = 4\pi R_{\rm abs} D_l$. This is in keeping with the nature of the WF approximation which always gives a lower bound to the exact solution [18]. Figure 4 gives calculated speed up factors, which are the ratios of calculated rate to the limiting rate $k = k_{\rm cap}(N)/k_{\rm cap}(1)$. With this scaling, the WF results are in good agreement with the simulation results.

C. Attractive potential as a tether proxy

Although it serves as an excellent approximation to the mean-force potential model, the hard-wall potential model serves as a poor quantitative approximation for the simulation and WF results for tethered capture, as indicated by the gray line in Fig. 4. Although the potential model captures the general shape of the simulation data, in that a sharp initial increase in rate is followed by more modest rate increases as the tether lengthens, the potential model fails to capture the true flatness of the plateau associated with the tether model. However, the simple analytic model does yield the control parameter, σ, which accurately captures the correct scale over which $k_{\rm cap}$ varies with tether length. This is shown in Fig. 4 with a vertical dashed line at the bond number associated with $\sigma^2 = 10$. For longer tethers, σ is comparable to 1, and the tether length dependence is much more modest. Overall, the potential model works as well as expected, considering previous simulations and

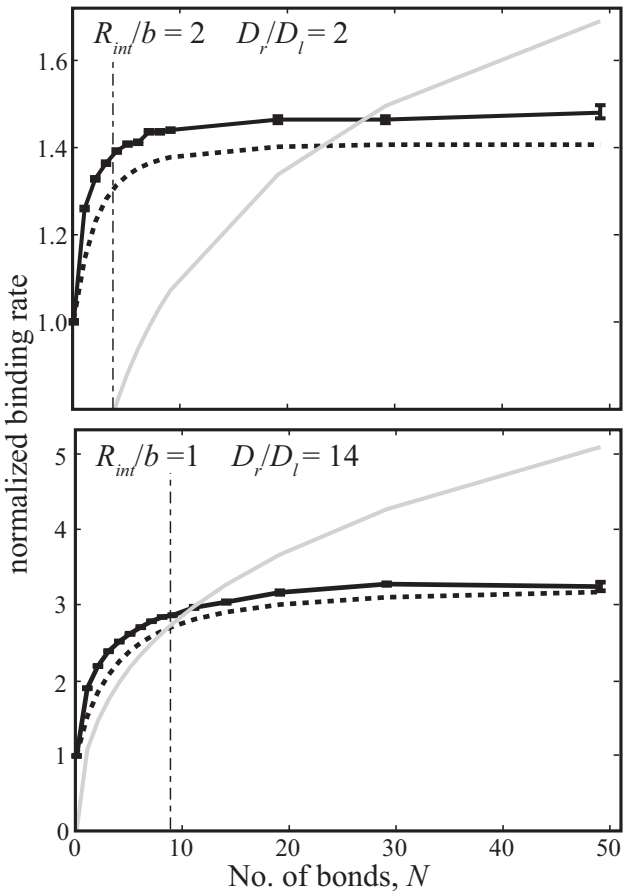

FIG. 4: Comparison of simulation to analytic approximations for two parameter sets. Simulation data (*black lines*), WF approximation results (*broken lines*), and effective potential results (*gray line*) are plotted as a function of tether length, which is expressed in number of beads, N. The WF results have been normalized to agree with k_{S} at $N = 1$. The root mean squared bond length is $b = 2$ and the ligand diffusion constant is $D_l = 0.005$ in simulation units. The vertical lines indicate the tether lengths at which the control parameter $\sigma^2 = 10$.

theory for polymer cyclization found mean-force potential models perform much worse than WF theory [29].

We have a good understanding of why the analytic model fails to reproduce the rates obtained in simulations at a quantitative level. For short polymers, Eq. 7 gives the Smoluchowski equation, $k_{\mathrm{cap}} = 4\pi D_l R$, where the radius of the absorbing sphere, R, is the polymer size. Contrast this to the correct no-tether limit, $k_{\mathrm{S}} = 4\pi D_l R_{\mathrm{abs}}$. This discrepancy is consistent with the violation of the assumption that the receptor can be modeled as a diffuse sink over a length scale similar to the size of the receptor itself. We also expect the mean-force

potential model to provide poor estimates in the long tether limit. We find the large R behavior by expanding around small values of σ, for which we recover the second order rate constant $k_{\text{cap}} = k_{\text{mix}}$. In this limit, c_r is spatially homogeneous, the tether applies no mean force, and the receptor diffuses freely. This is not a good approximation for polymer dynamics, which are not diffusive (see Appendix D and Ref. [19]). The model agrees best with simulation for small interaction radii, $R_{\text{abs}} < b$, a behavior consistent with the assumptions outlined in Section A.

IV. TETHER PROPERTIES AFFECT THE CAPTURE RATE

Although the analytic solution, Eq. 7, suffers from poor quantitative agreement with simulation, it provides physical intuition about the tethered binding model which does not clearly emerge from the WF approach. Equation 7 suggests that $\sigma^2 \approx k_{\text{mix}}/RD_l$ is a dimensionless parameter that controls the behavior of the tethered-capture reaction. Namely, it describes how "opaque" the region confining the receptor is to the ligand. The physical meaning of the opacity becomes clear once we recognize that it is the ratio of two time scales, $\tau_D = R^2/D_l$, the characteristic time for the ligand to diffuse over a sphere with radius R, and $\tau_R = \frac{4}{3}R^3/k_{\text{mix}}$, which is the characteristic binding time for ligands to the receptor at a concentration of one ligand per sphere volume. As σ^2 approaches zero, the ligand moves freely through the region and there is little interaction, whereas as σ^2 approaches infinity, every ligand that enters the confinement region reacts with the receptor.

By expanding k_{cap} around small values of σ in Eq. 7, we find the regime in which the reaction rate is dependent on R, the size of the confinement region. Recall that R is determined by both the flexibility of the polymer via b, the length of one statistical segment, and the total length of the polymer, Nb. For $\sigma^2 \ll 1$, the leading order term dominates, and the rate is independent of R. However, for values of $\sigma^2 > 1$, the second order term becomes significant, and the reaction rate k_{cap} is sensitive to tuning the size of the confinement region. These qualitative characteristics of the two regimes are confirmed by the WF results and by simulations.

A. Role of tethering motifs in biology

Tethering motifs are common in biology, as discussed in the Introduction where several examples were given in which tethering receptors may regulate reaction rates. We have shown that polymer characteristics are important in determining diffusion-limited reaction rates, and we suggest that tuning polymer parameters can be used to regulate kinetic rates in some natural and synthetic systems.

To that end, we apply the dimensionless control parameter σ^2 to predict whether tether length and flexibility are important parameters in determining the steady-state diffusion-limited binding rates. Table I gives estimates of σ^2 for a few example systems. As we mention below, $\sigma^2 \ll 1$ for formins, indicating a lack of sensitivity to polymer characteristics in the tethered-capture rate $k_{\rm cap}$ [27, 30, 31]. In contrast, we estimate $\sigma^2 \gg 1$ for free avidin binding to biotin molecules tethered by polyethylene glycol (PEG) to a microscope slide. The biotin-avidin association rate $k_{\rm cap}$ should depend strongly upon the length of the PEG tether [32]. For viral capsid subunits binding ssRNA and for the protein Est1p binding telomerase RNA we estimate $\sigma^2 \approx 1$ [7, 33]. For these two examples, our theory predicts that the respective binding rates show modest dependence, by at most a factor of two, on RNA tether length.

TABLE I: Sensitivity of tethered-capture rate to polymer properties of the tether in various systems.

system	interaction	σ^2	tether influence
wild-type formins	profilin-actin binding FH1 binding sites	$\ll 1$	none
polymer coated surfaces	avidin binding PEG-tethered biotin	$\gg 1$	strong
viral capsid assembly	capsid subunits binding ssRNA molecules	≈ 1	weak
yeast telomerase RNA	Est1p binding RNA telomerase arm	≈ 1	weak

In conclusion, we have shown how confining reactants by tethers affects reaction rates. Under certain conditions, the tethered-capture rate is sensitive to the length and flexibility of the tether. We suggest that natural and synthetic systems, such as formins and surface-tethered receptors, can exploit this sensitivity to control reaction rates.

V. ACKNOWLEDGMENTS

The authors thank Bruce Goode, Chris Gould, Rob Phillips, and David Van-Valen for their contributions. This work is supported by National Science Foundation grant No. DMR-0706458, No. DGE-0549390, and the MRSEC No. 0820492 at Brandeis University.

Appendix A: Validity of applying the mean-force potential

Applying a mean-force potential to study reactions involving polymer dynamics, i.e. assuming the local equilibrium approximation (LEA), is valid if the polymer relaxes much faster than the reaction of interest occurs [20, 29]. When a reaction is at steady state, there is no finite timescale for comparisons, but we will show that LEA holds in steady state if it also holds for the corresponding time-dependent reaction in which the source term for the ligands is absent, and their concentration decays over time.. We focus on the end-to-end vector of a polymer in the presence of a sink, for which we write the exact expression,

$$\partial_t G(\mathbf{r}, t; \mathbf{r}_0, t_0) = \mathcal{D}\left[G(\mathbf{r}, t; \mathbf{r}_0, t_0)\right] - S(\mathbf{r}) G(\mathbf{r}, t; \mathbf{r}_0, t_0), \tag{A1}$$

where $G(\mathbf{r}, t; \mathbf{r}_0, t_0)$ is the Green's function for the end-to-end vector $\mathbf{r}$ initially at $\mathbf{r}_0$, $\mathcal{D}$ is the propagator that characterizes the diffusive motion of the polymer, and $S(\mathbf{r})$ is the sink function that defines the spatial extent of the interaction. We also write the approximate equation

$$\partial_t \bar{G}(\mathbf{r}, t; \mathbf{r}_0, t_0) = \mathcal{D}_{\mathrm{mf}}\left[\bar{G}(\mathbf{r}, t; \mathbf{r}_0, t_0)\right] - S(\mathbf{r}) \bar{G}(\mathbf{r}, t; \mathbf{r}_0, t_0), \tag{A2}$$

where $\mathcal{D}_{\mathrm{mf}}$ is the diffusion operator corresponding to free diffusive motion in a mean-force potential and $\bar{G}$ is the Green's function that solves this modified equation. LEA asserts that if the mean decay time of the Green's function G in the presence of the sink S is longer than the relaxation time of G (in the *absence* of the sink), then $\bar{G} \approx G$ at long times. To produce steady-state solutions to the above equations, we introduce a set of sources defined by the function $K(\mathbf{r})$ and set the time derivative to zero:

$$\begin{aligned} 0 &= \mathcal{D}(G_{\mathrm{ss}}) - S(\mathbf{r}) G_{\mathrm{ss}} + K(\mathbf{r}) \\ 0 &= \mathcal{D}_{\mathrm{mf}}(\bar{G}_{\mathrm{ss}}) - S(\mathbf{r}) \bar{G}_{\mathrm{ss}} + K(\mathbf{r}). \end{aligned} \tag{A3}$$

The steady-state solutions, G_{ss} and $\bar{G}_{\mathrm{ss}}$, are related to the Green's functions by

$$G_{\mathrm{ss}} = \iint_0^\infty G(\mathbf{r}, t; \mathbf{r}_0, t_0) K(\mathbf{r}_0)\, dt\, d\mathbf{r}_0 \tag{A4}$$

and identically for $\bar{G}_{\rm ss}$, where the spatial integral is over all $\mathbf{r}_0$. It is now clear that if $\bar{G}$ is a good approximation for G over our time scale of interest, then $\bar{G}_{\rm ss}$ is a good approximation for $G_{\rm ss}$.

We apply the general result above to our coupled ligand-receptor diffusion system given by the time dependent Eq. 2. The relevant decay time τ_d is that of c_r and c_l in the presence of the interaction term $k_{\rm mix}c_rc_l$. Although this time scale depends on the initial and boundary conditions, we estimate a lower limit by taking the shorter of $(k_{\rm mix}C_0)^{-1}$ and $(k_{\rm mix}c_r')^{-1}$, where c_r' corresponds to one receptor within a sphere of radius $\langle R_{\rm ee}\rangle$, the mean end-to-end distance of the polymer. In the dilute limit, where the inter-ligand spacing is much greater than the size of the polymer, the latter time is shorter, so we let $\tau_d \approx \langle R_{\rm ee}\rangle^3/k_{\rm mix}$. Therefore, LEA holds if the relaxation time of the polymer,

$$\tau_r \ll \frac{\langle R_{\rm ee}\rangle^3}{k_{\rm mix}}. \tag{A5}$$

Using Eq. A5 and the scaling relations for the relaxation time and end-to-end distance for a bead-spring chain[19], $\tau_r \sim N^{(1+2\nu)}b^2D_r^{-1}$ and $R_{\rm ee} \sim N^\nu b$, we obtain for an ideal chain ($\nu = 1/2$) a validity condition for LEA,

$$N^{1/2}\frac{R_{\rm abs}}{b}\frac{(D_r + D_l)}{D_r} \ll 1. \tag{A6}$$

Thus, the Local Equilibrium Approximation holds for sufficiently short tethers and very inflexible tethers. As an example of the applicability to biological systems, we expect LEA to apply to formins with tethers of fewer than about 30 amino acids using parameters found in [15] and references therein.

Appendix B: Decoupling approximation

Using scaling arguments, we can derive the conditions under which Eq. 2, which describes the time evolution of the receptor concentration, c_r, does not depend on the ligand concentration c_l. We fist observe that since interactions deplete both ligands and receptors, and far away from the reaction c_l is constant whereas c_r vanishes, the solution to Eq. 2 must have c_l increase and c_r decrease over all distances r from the tether anchor. We can therefore define a region of characteristic size R in which the receptor is bound such that

$$\int_0^R c_r(r)4\pi r^2 dr > \int_R^\infty c_r(r)4\pi r^2 dr. \tag{B1}$$

Using these criteria, we estimate the size of terms in Eq. 2 when r is on the order of R. We note that c_r scales as R^{-3} and c_l scales as C_0, the far-field ligand concentration. From the boundedness of the interaction, the nth derivatives of c_r and c_l scale as R^{-3-n} and $C_0 R^{-n}$, respectively. Assuming a quadratic tethering force $\nabla U \sim wr$, where U is in units of $k_{\mathrm{B}}T$, Eq.2 can be rewritten as

$$\begin{aligned} k_{\mathrm{mix}} R^{-3} c_r c_l &\sim \frac{D_l}{R^2} \nabla^2 c_l \\ k_{\mathrm{mix}} C_0 c_l c_r &\sim \frac{D_r}{R^2} \nabla^2 c_r + w D_r (c_r + \frac{r}{R} \partial_r c_r), \end{aligned} \tag{B2}$$

where c_r and c_l are rescaled functions of order unity.

For a sufficiently weak coupling strength k_{mix}, the distribution c_r is determined by the tethering force alone, and not by interactions with c_l. This regime, in which the left-hand side of Eq. B2 can be ignored, is described by

$$C_0 \ll \frac{D_r w}{k_{\mathrm{mix}}}, \tag{B3}$$

which provides a necessary condition for the decoupled system to accurately approximate the coupled system. For larger coupling strengths, or larger ligand concentrations, if the decoupled system continues to provide a decent approximation for the full system, Eq. B3 continues to hold. Therefore, although we have not estimated the error introduced by decoupling, we have derived a criterion for self-consistency. It provides a good estimate of favorable conditions for decoupling, which are supported by explicit calculations that retain the interaction term, such as those shown in Fig. 3. Note that the relationship will always hold for sufficiently low ligand concentration.

Appendix C: Monte-Carlo Polymer Simulation Methods

We simulate the interactions between free ligands and a tethered receptor using off-lattice Monte-Carlo dynamics. The polymer consists of N beads, the last being the receptor. The beads are connected by harmonic springs with energies $E_n = 3(\mathbf{x}_n - \mathbf{x}_{n-1})^2/2b^2$, where $\mathbf{x}_n$ is the location of the nth bead; the thermal energy $k_{\mathrm{B}}T = 1$. The polymer is anchored to the center of a simulation box with periodic boundary conditions, and the box is filled with ligands. At each time step, ligands move small steps in each dimension such that their mean-square displacement after t steps is $6D_l t$. The beads which make up the polymer attempt small moves in each direction, and are accepted according to the Metropolis criterion [34].

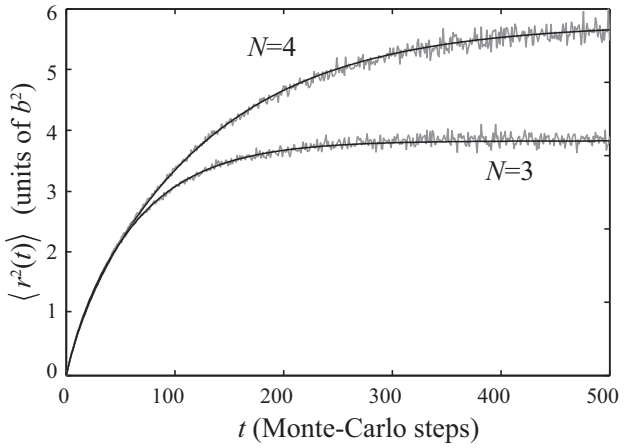

FIG. 5: Diffusion of a polymer tether. Simulations of a polymer model (*gray line*) are used to compute the mean square displacement of the terminal monomer, plotted in units of b^2 versus Monte-Carlo steps. These data are compared to analytic results (*black line*) based on the Rouse model of polymer dynamics (Eq. D34). The comparison serves as a check on the validity of the simulations and as a way of estimating the diffusion constant of the simulated polymer. We show results for two polymer lengths calculated using a Kuhn length of $b = 6.3$ trial steps. The resulting diffusion constant is $D_r = 0.0138$ in units of b^2/mcs.

To confirm that the simulation recreates Rouse dynamics with the Monte-Carlo step as a unit of time, we measure the mean-square displacement of the terminal node, $\langle \mathbf{r}_r^2(t) \rangle = \langle [\mathbf{r}_r(t_0 + t) - \mathbf{r}_r(t_0)]^2 \rangle$, where the average is over starting times, t_0. With this measurement we also calculate the diffusion constant D_r of the terminal bead when disconnected from the rest of the polymer by performing a least squares fit to Eq. 12 (for example, see Fig. 5). These measurements are repeated for each value of N, b, and step size because the move acceptance ratio varies with these parameters.

When a ligand is within the interaction distance $R_{\rm abs}$ of the terminal bead, it is absorbed and replaced randomly at the edge of the simulation box of size $R_{\rm sim}$, so as to keep the ligand concentration in the far-field fixed. Initially, M ligands are distributed throughout the box and the beads are placed, starting with the anchored bead at the origin, by randomly generating $N - 1$ bonds. We initialize the simulation by allowing the polymer bonds to decorrelate, and by waiting for the ligand concentration in the box to approach steady state. Over several million time steps, we measure both the mean collision rate, $k_{\rm sim}$, and the ligand concentration in a shell of radius $R_{\rm sim}$, $C(R_{\rm sim})$. We find the effective concentration

of ligands infinitely far away, C_0, by equating the absorption rate inside the sphere, k_{sim}, with the diffusive flux through the sphere, $4\pi R_B D_l(C_0 - C(R_{\text{sim}}))$. We solve for C_0, and write the second order rate constant, $k_{\text{cap}} = k/C_0$ as

$$k_{\text{cap}} = \left(\frac{C(R_B)}{k} + \frac{1}{4\pi R_B D_l} \right)^{-1}. \tag{C1}$$

Equation C1 relates the measured quantities $C(R_B)$ and k to the sought rate constant.

Appendix D: Dynamics of an anchored discrete finite bead-spring chain

In this appendix, we find the dynamics of a bead-spring chain, consisting of N beads connected by $N-1$ harmonic springs. The chain is anchored at one end. In particular, we find the mean squared displacement as a function of time of the terminal bead, and the end-to-end vector time-dependent correlation functions. To solve this problem, we express the dynamics of each bead with a Langevin equation, and then express the system of equations in terms of the bond vectors between beads. The coupling between bonds can be expressed as a nearly diagonal matrix, which we diagonalize by finding its eigenvalues and eigenvectors. This amounts to decomposing the configuration of the system into $N-1$ normal modes.

Each of the normal modes follows an independent Langevin equation for diffusion in a harmonic well, for which the dynamics are well known. Before applying those results, the functions that characterize the noise must be expressed in the new basis, and their autocorrelation functions computed. Finally, we express the bond vectors, and thus the end-to-end vector, as combinations of normal modes, each of which has well characterized dynamics. Thus we can express functions of the end-to-end vector as sums over $N-1$ normal modes.

The scope of our approach is different from those found in sources such as Doi and Edwards [19], and Edwards [18], in three critical respects. First, we never assume large N in our results, so the results are valid for short chains. Second, we do not take the continuum limit of infinite bond number, but rather leave the bonds discrete. Therefore, the modes are found by linearizing a system of coupled differential equations, each describing a different bond, rather than finding normal modes of a single bounded differential equation. Third, we anchor one end of the polymer. In this way, our treatment differs from Lin [28]. Of course, the price we pay for exactness and generality is loss of simplicity. We must perform a sum

over all N modes, which is cumbersome for large N. We pay in computation of long chains for what we gain in exactness of short chains, which leads to excellent agreement with our simulations in which $N \leq 50$.

Decomposition into normal Rouse modes

Langevin dynamics in real space

Due to the spring forces connecting beads in the chain, the time derivative of the location, $\mathbf{R}_n$, of the nth bead depends upon the location of its neighbors. Therefore, the location of the internal beads ($n = 1$ through $n = N - 1$) follow the Langevin equation

$$\frac{\mathrm{d}\mathbf{R}_n}{\mathrm{d}t} = -\frac{3k_BT}{\xi b^2}(2\mathbf{R}_n - \mathbf{R}_{n+1} - \mathbf{R}_{n-1}) + g_n(t), \tag{D1}$$

where b is the bond length, k_B is Boltzmann's constant, T is temperature, and ξ is the friction coefficient of each bead. The locations of the anchored bead and the bead at the free end follow

$$\frac{\mathrm{d}\mathbf{R}_1}{\mathrm{d}t} = \mathbf{R}_1 = 0 \tag{D2}$$

$$\frac{\mathrm{d}\mathbf{R}_N}{\mathrm{d}t} = -\frac{3K_BT}{\xi b^2}(\mathbf{R}_N - \mathbf{R}_{N-1}) + g_n(t). \tag{D3}$$

The function $g_n(t)$ represents the thermal noise to the nth bead. It has a Gaussian distribution, which we express as the mean and variance

$$\langle g_n(t)\rangle = 0 \tag{D4}$$

$$\langle g_{n\alpha}(t) g_{m\beta}(t')\rangle = \frac{2K_BT}{\xi}\delta_{nm}\delta_{\alpha\beta}\delta(t-t'), \tag{D5}$$

where $g_{n\alpha}$ is the component of g_n along dimension α.

We next define bond vectors as $\mathbf{b}_n = \mathbf{R}_{n+1} - \mathbf{R}_n$, and rewrite the time derivatives of $\mathbf{R}$ in terms of $\mathbf{b}_n$. The components of $\mathbf{b}_n$ in each dimension evolve independently, so to simplify notation, we treat only one dimension. The bond vector $\mathbf{b}_n$ evolves according to

$$\frac{d\mathbf{b}_s}{dt} = -\frac{3K_BT}{\xi b^2}\sum_{t=1}^{N-1} A_{st}\mathbf{b}_t + (g_{s+1}(t) - g_s(t)), \tag{D6}$$

where $g_1 = 0$ because the first bead is anchored. The Rouse matrix A describes the coupling between bonds:

$$A = \begin{pmatrix} 1 & -1 & 0 & 0 & . & 0 & 0 \\ -1 & 2 & -1 & 0 & . & 0 & 0 \\ 0 & -1 & 2 & -1 & . & . & . \\ . & . & . & . & . & . & . \\ . & . & . & . & 2 & -1 & 0 \\ 0 & 0 & . & . & -1 & 2 & -1 \\ 0 & 0 & . & . & 0 & -1 & 2 \end{pmatrix}. \tag{D7}$$

Equation $D6$, with the form of matrix A, fully describes the dynamics of the bead-spring chain in real space. In the following sections we decompose the chain's motion into its eigenmodes, and work in the eigenspace to find statistics of the chain's motion.

Finding the eigenvalues

We diagonalize A by finding the eigenvalues λ_p and eigenvectors $\mathbf{c}_p$ that satisfy the eigenvalue equation $A\mathbf{c}_p = \lambda_p \mathbf{c}_p$. The $z = N-1$ eigenvalues are found by setting the determinant $D_z = |A - \lambda I_z| = 0$, where I is the $z \times z$ identity matrix, and solving for λ. If we define $x = \lambda - 2$, the determinant is

$$D_z = \begin{vmatrix} x+1 & 1 & 0 & 0 & \cdots \\ 1 & x & 1 & 0 & \cdots \\ 0 & 1 & x & 1 & \cdots \\ 0 & 0 & 1 & x & \cdots \\ & & & & \ddots \end{vmatrix}, \tag{D8}$$

where the size of the matrix D_z is $z = N-1$. The determinants are described by difference equations (as in [28]) and two boundary values as follows:

$$\begin{aligned} D_z &= xD_{z-1} - D_{z-2} \\ D_1 &= x + 1 \\ D_2 &= x^2 + x - 1. \end{aligned} \tag{D9}$$

Solution for x, given these difference equations, are of the form $x = 2\cos(\theta) = \exp(i\theta) + \exp(-i\theta)$. Therefore, a solution to D_z can be written as

$$D_z = B_1 \exp(i\theta) + B_2 \exp(-i\theta), \tag{D10}$$

where B_1 and B_2 are constants. We apply the boundary values for D_1 and D_2 to find the constants B_1 and B_2:

$$B_1 = \frac{\exp(i\theta) + 1}{\exp(i\theta) - \exp(-i\theta)} \quad B_2 = \frac{-\exp(-i\theta) - 1}{\exp(i\theta) - \exp(-i\theta)}. \tag{D11}$$

We next apply the requirement for eigenvalues, $D_z = 0$, to Eq. D10. Algebraic manipulation with trigonometric identities yields the relation $\sin[(z+1)\theta] = -\sin[z\theta]$. This, in turn, requires θ to take the values,

$$\theta = \frac{2p\pi}{2z+1} \quad p = 1, 2, ..., z. \tag{D12}$$

These values for θ correspond to the eigenvalues

$$\lambda_p = 4\cos^2\left[\frac{p\pi}{2N-1}\right] \quad p = 1, 2, ..., (N-1)\ . \tag{D13}$$

It turns out to be useful to redefine the mode index p by changing variables: $p \to N - p$. Now the eigenvalues are,

$$\lambda_p = 4\cos^2\left[\frac{(N-p)\pi}{2N-1}\right] \tag{D14}$$

$$= 2 + 2\cos\left[\frac{2N\pi}{2N-1} - \frac{2p\pi}{2N-1}\right] \tag{D15}$$

$$= 4\sin^2\left[\frac{\pi(2p-1)}{2(2N-1)}\right] \quad p = 1, 2, ..., (N-1)\ . \tag{D16}$$

Finding the normal modes

We now find the eigenvectors $\mathbf{c}_p$ associated with each eigenvalue λ_p by solving the eigenvalue equation $A\mathbf{c}_p = \lambda_p \mathbf{c}_p$, where c_{pk} is the kth component of the pth Rouse mode (where $1 \le k \le N-1$). The form of the matrix A then gives rise to another set of difference equations over the components of $\mathbf{c}_p$, with boundary values:

$$\begin{aligned} c_{k+1} + c_{k-1} &= (2 - \lambda_p)c_k \\ c_2 &= (1 - \lambda_p)c_1 \\ c_{N-2} &= (2 - \lambda_p)c_{N-1}, \end{aligned} \tag{D17}$$

where we have suppressed the subscript p on the eigenvectors for ease of reading. Eqs. D17 are satisfied by the solution

$$c_k = B_1 \exp\left[\frac{i(2p-1)k\pi}{2N-1}\right] + B_2 \exp\left[\frac{-i(2p-1)k\pi}{2N-1}\right]. \tag{D18}$$

The boundary conditions requires

$$B_2 = B_1 \exp\left[\frac{i(2p-1)\pi}{2N-1}\right]. \tag{D19}$$

To make the eigenvector decomposition orthonormal, we apply the normalization condition $\sum_{k=1}^{N-1} c_k^* c_k = 1$, and find that $|B_1|^2 = 1/(2N-1)$. By writing the constant B_1 in the following form,

$$B_1 = \frac{1}{\sqrt{2N-1}} \exp\left[\frac{-i(2p-1)\pi}{2(2N-1)}\right], \tag{D20}$$

the kth component of the pth eigenvector can be written in the convenient form,

$$c_{pk} = \frac{2}{\sqrt{2N-1}} \cos\left[\frac{(2p-1)(2k-1)\pi}{2(2N-1)}\right]. \tag{D21}$$

Finally, we write a transformation between the bond vectors (projected in each dimension) in real space and in eigenspace,

$$\mathbf{b}_k = \sum_{p=1}^{N-1} c_{ps}\mathbf{q}_p, \tag{D22}$$

where $\mathbf{q}_p$ is the magnitude of the pth normal mode contribution, and its components are along the three dimensions. We can express this transformation using the transformation matrix, C, composed of the values c_{pk}: $\mathbf{b}_\alpha = C\mathbf{q}_\alpha$. The columns of C are the normal modes written in real bead space representation.

The Langevin equation in Rouse space

By substituting Eq. D22 into the Langevin equation, we write it as diffusion of each normal mode:

$$\frac{d\mathbf{q}_p}{dt} = \frac{-3K_BT}{\xi b^2} \sum_{k,t,u=1}^{N-1} c_{kp}A_{kt}c_{tu}\mathbf{q}_u + \mathbf{h}_p(t) \tag{D23}$$

where $\mathbf{h}_p(t) = \sum_{k=1}^{N-1} c_{kp}(g_{k+1}(t) - g_k(t))$. Because the eigenvector decomposition is orthonormal, we have $\sum_{t=1}^{N-1} c_{tk}c_{tu} = \delta_{ku}$. Therefore, we can rewrite the Langevin equation for each mode as a simple harmonic oscillator:

$$\frac{d\mathbf{q}_p}{dt} = \frac{-3K_BT}{\xi b^2}\lambda_p\mathbf{q}_p + \mathbf{h}_p(t). \tag{D24}$$

To find the dynamical behavior of $\mathbf{q}_p(t)$, we first find the dynamical behavior of $\mathbf{h}_p(t)$. We know that $\langle \mathbf{h}_p(t) \rangle = 0$, but we must also find its autocorrelation function, $\langle h_{p\alpha}(t)h_{p\beta}(t') \rangle$,

where α, β are dimensional indices. We first expand the autocorrelation as

$$\langle h_{p\alpha}(t)h_{q\beta}(t')\rangle = \left\langle \sum_{k=1}^{N-1} c_{kp}(g_{k+1,\alpha} - g_{k,\alpha}) \sum_{t=1}^{N-1} c_{tq}(g_{t+1,\beta} - g_{t,\beta}) \right\rangle. \tag{D25}$$

Using the properties of the noise functions $g_k(t)$, and noting that $g_N = 0$, we find that

$$\langle h_{p\alpha}(t)h_{q\beta}(t')\rangle = \frac{2K_BT}{\xi}\delta(t-t')\delta_{pq}\left[\sum_{k=1}^{N-1} c_{kp}c_{kp} + \sum_{k=2}^{N-1} c_{kp}c_{kp} - 2\sum_{k=1}^{N-2} c_{k+1,p}c_{k,p}\right]. \tag{D26}$$

Performing the sums over the transformation matrices, as defined in Eq. D21, we apply algebraic manipulations to find the autocorrelation function,

$$\langle h_{p\alpha}(t)h_{q\beta}(t')\rangle = \frac{12K_BT}{\xi}\delta_{pq}\delta_{\alpha\beta}\delta(t-t')\left[1 - \cos\left(\frac{(2p-1)\pi}{2N-1}\right)\right]. \tag{D27}$$

Relaxation of Rouse modes

Thus far, we have found the eigenvalues, λ_p, the transform matrix between the eigenspace and real space, C, and the noise correlations in eigen-space. Above, we noted that the Langevin equation for each mode was that of a harmonic oscillator. Therefore, we express the relaxation of each Rouse mode as that of a harmonic oscillator [19],

$$\langle \mathbf{q}_p(t)\mathbf{q}_q(0)\rangle = \int_{-\infty}^{t}\int_{-\infty}^{0} \mathrm{d}t'\mathrm{d}t'' \exp\left(\frac{-(t-t'-t'')}{\tau_p}\right)\langle h_{p\alpha}(t')h_{p\beta}(t'')\rangle\delta_{pq}, \tag{D28}$$

where the relaxation time of the pth normal mode is

$$\tau_p = \frac{\xi b^2}{3K_BT\lambda_p} = \frac{\xi b^2}{12K_BT\sin^2\left(\frac{\pi(2p-1)}{2(2N-1)}\right)}. \tag{D29}$$

Note that the relaxation of the slowest $p = 1$ mode approaches $\tau_1 \approx \frac{4\xi b^2 N^2}{3K_BT\pi^2}$, in the limit of large N. This agrees with the continuous, $N \to \infty$ result found in, for example, Doi and Edwards [19]. To finish the calculation, we substitute the noise correlation function into Eq. D28, evaluate the integrals, and apply algebraic manipulations to the result. This yields the autocorrelation function of each Rouse mode:

$$\langle \mathbf{q}_{p\alpha}(t)\mathbf{q}_{q\beta}(0)\rangle = \delta_{pq}\delta_{\alpha\beta}b^2e^{-t/\tau_p}. \tag{D30}$$

Results in real space

We next find statistical quantities in real space such as the end-to-end autocorrelation function and mean squared displacement of the terminal bead. The location of the terminal bead in each dimension can be written as a sum over all the bond vectors,

$$\mathbf{R} = \sum_{k=1}^{N-1} \mathbf{b}_k(t) = \sum_{k=1}^{N-1}\sum_{p=1}^{N-1} c_{kp}\mathbf{q}_p(t).$$

First we write $R(t)$ as a sum over Rouse modes, again using Eq. D21, several trigonometric identities, and the integer nature of N and p:

$$\begin{aligned}\mathbf{R}(t) &= \sum_{p=1}^{N-1} \frac{2}{\sqrt{2N-1}}\mathbf{q}_p(t) \sum_{k=1}^{N-1} \cos\left[\frac{(2p-1)(2k-1)\pi}{2(2N-1)}\right] \\ &= \sum_{p=1}^{N-1} \frac{-1^{p+1}}{\sqrt{2N-1}}\,\mathbf{q}_p(t) \cot\left[\frac{(2p-1)\pi}{2(2N-1)}\right]. \end{aligned} \tag{D31}$$

The time autocorrelation function of the end-to-end vector is,

$$\begin{aligned}\langle \mathbf{R}(t)\mathbf{R}(0)\rangle &= \frac{4}{2N-1}\sum_{k=1}^{N-1}\sum_{p=1}^{N-1} \cos\left[\frac{(2k-1)(2p-1)\pi}{2(2N-1)}\right] \times \\ &\qquad \times \sum_{m=1}^{N-1}\sum_{n=1}^{N-1} \cos\left[\frac{(2m-1)(2n-1)\pi}{2(2N-1)}\right] \langle \mathbf{q}_p(t)\mathbf{q}_n(0)\rangle \\ &= \sum_{p=1}^{N-1} \frac{b^2}{2N-1} \cot^2\left[\frac{(2p-1)\pi}{2(2N-1)}\right] e^{-t/\tau_p}, \end{aligned} \tag{D32}$$

where we have applied Eq. D30 and various trigonometric identities.

We next find the mean squared displacement of the terminal bead as a function of time, $\phi = \langle(\mathbf{R}(t) - \mathbf{R}(0))^2\rangle$, in a similar fashion. Now we can solve for ϕ:

$$\phi = \langle \mathbf{R}(t)^2\rangle + \langle \mathbf{R}(0)^2\rangle - 2\langle \mathbf{R}(t)\mathbf{R}(0)\rangle \tag{D33}$$

$$= \sum_{p=1}^{N-1} \frac{2b^2}{2N-1} \cot^2\left[\frac{(2p-1)\pi}{2(2N-1)}\right](1 - e^{-t/\tau_p}). \tag{D34}$$

In Appendix C, we compare this formula to the results of Monte Carlo simulations and find excellent agreement.

---

[1] J. Yan and J. F. Marko, Phys. Rev. Lett. **93**, 108108 (2004).

[2] B. Windisch, D. Bray, and T. Duke, Biophys. J. **91**, 2383 (2006).

[3] C. Z. Zhang and Z. G. Wang, Langmuir **23**, 13024 (2007).

[4] V. M. Krishnamurthy, V. Semetey, P. J. Bracher, N. Shen, and G. M. Whitesides, J. Am. Chem. Soc. **129**, 1312 (2007).

[5] D. Van Valen, M. Haataja, and R. Phillips, Biophys. J. **96**, 1275 (2009).

[6] T. Hu and B. I. Shklovskii, Physical Review E **76**, (2007).

[7] D. C. Zappulla and T. R. Cech, Proc Natl Acad Sci U S A **101**, 10024 (2004).

[8] G. Longo and I. Szleifer, Langmuir **21**, 11342 (2005).

[9] C. Jeppesen, J. Y. Wong, T. L. Kuhl, J. N. Israelachvili, N. Mullah, S. Zalipsky, and C. M. Marques, Science **293**, 465 (2001).

[10] A. G. Moreira and C. M. Marques, J Chem Phys **120**, 6229 (2004).

[11] J. Martin, C. Z. Zhang, and Z. G. Wang, Journal of Polymer Science: Part B: Polymer Physics (2006).

[12] C. J. G. J. Friedman, L. J., Biophys J **91**, 1023 (2006).

[13] O. G. Berg, R. B. Winter, and P. H. von Hippel, Biochemistry **20**, 6929 (1981).

[14] B. L. Goode and M. J. Eck, Annual Review of Biochemistry **76**, 593 (2007).

[15] D. Vavylonis, D. R. Kovar, B. O'Shaughnessy, and T. D. Pollard, Mol Cell **21**, 455 (2006).

[16] P. E. J. Rouse, J Chem Phys **21** (1953).

[17] G. Wilemski and M. Fixman, The Chem Phys **60** (1974).

[18] M. Doi, Chemical Physics **11**, 107 (1975).

[19] M. Doi and E. S. F., *The Theory of Polymer Dynamics* (Clarendon Press, 1988).

[20] A. Szabo, K. Schulten, and Z. Schulten, J Chem Phys **72**, 4350 (1980).

[21] N. M. Toan, G. Morrison, C. Hyeon, and D. Thirumalai, J Phys Chem B **112**, 6094 (2008).

[22] J. Keizer, Chem. Rev. **87**, 167 (1987).

[23] G. Adam and M. Delbruck, Structural chemistry and molecular biology **198** (1968).

[24] O. Bénichou, D. Grebenkov, P. Levitz, and C. Loverdo, Physical review letters (2010), URL `http://link.aps.org/doi/10.1103/PhysRevLett.105.150606`.

[25] T. Frembgen-Kesner and A. Elcock, Biophysical journal **99**, L75 (2010), URL `http://linkinghub.elsevier.com/retrieve/pii/S0006349510011033`.

[26] S. Northrup and H. Erickson, Proceedings of the National Academy of Sciences of the United States of America **89**, 3338 (1992), URL `http://www.pnas.org/content/89/8/3338.short`.

[27] D. R. Kovar, E. S. Harris, R. Mahaffy, H. N. Higgs, and T. D. Pollard, Cell **124**, 423 (2006).

[28] Y. H. Lin, *Polymer viscoelasticity: basics, molecular theories, and experiments* (World Scientific, River Edge, 2003).

[29] R. W. Pastor, R. Zwanzig, and A. Szabo, J Chem Phys **105**, 3878 (1996).

[30] T. H. Evers, E. M. van Dongen, A. C. Faesen, E. W. Meijer, and M. Merkx, Biochemistry **45**, 13183 (2006).

[31] K. S. Zaner, R. G. King, J. Newman, K. L. Schick, R. Furukawa, and B. R. Ware, J Biol Chem **263**, 7186 (1988).

[32] R. Bhat and S. N. Timasheff, Protein science : a publication of the Protein Society **1**, 1133 (1992), ISSN 0961-8368, URL `http://www.pubmedcentral.nih.gov/articlerender.fcgi?artid=2142180\&tool=pmcentrez\&rendertype=abstract`.

[33] B. Tinland, A. Pluen, and J. Sturm, Macromolecules **9297**, 5763 (1997), URL `http://pubs.acs.org/doi/abs/10.1021/ma970381\%2B`.

[34] N. Metropolis, A. W. Rosenbluth, M. N. Rosenbluth, A. H. Teller, and E. Teller, J Chem Phys **21** (1953).